

# New candidate planetary nebulae in M 81<sup>\*</sup>

Laura Magrini<sup>1</sup>, Mario Perinotto<sup>1</sup>, Romano L.M. Corradi<sup>2</sup>, Antonio Mampaso<sup>3</sup>

<sup>1</sup> Dipartimento di Astronomia e Scienza dello Spazio, Università di Firenze, L.go E. Fermi 5, I-50125 Firenze, Italy

<sup>2</sup> Isaac Newton Group of Telescopes, Apartado de Correos 321, 38700 Santa Cruz de La Palma, Canarias, Spain

<sup>3</sup> Instituto de Astrofísica de Canarias, c. Vía Láctea s/n, 38200, La Laguna, Tenerife, Canarias, Spain

received date; accepted date

**Abstract.** A  $34' \times 34'$  field centred on the spiral galaxy M 81 has been searched for emission-line objects using the prime focus wide field camera (WFC) of the 2.54 m Isaac Newton Telescope (La Palma, Spain). A total of 171 candidate planetary nebulae (PNe) are found, 54 of which are in common with the ones detected by Jacoby et al. (1989). The behaviour of PNe excitation as a function of galactocentric distance is examined, and no significant variations are found. The PNe luminosity function is built for the disk and bulge of M 81, separately. A distance modulus of  $27.92 \pm 0.23$  mag is found for disk PNe, in good agreement with previous distance measurements for M 81 (Jacoby et al. 1989; Huterer et al. 1995).

**Key words:** Planetary nebulae – Galaxies: M81 – Galaxies: ISM

## 1. Introduction

Basic information about planetary nebulae (PNe) in external galaxies has been summarized by Jacoby (1997). Many hundreds of PNe were discovered in spiral galaxies (mainly in M 31), in irregular (LMC and SMC) and elliptical galaxies up to the distance of the Virgo cluster. More recently, 131 candidate PNe have been discovered by Magrini et al. (2000, 2001) in M 33. PNe are important objects in the study of stellar population of intermediate age in galaxies of different morphological types and in different chemical environments, and in the assessment of the kinematical properties of all morphological components of galaxies (disks, bulges, haloes).

M 81 (NGC 3031), a nearby galaxy outside the Local Group, belongs to the group of the most massive spiral galaxies (SAab) being also the nearest LINER galaxy. Together with M 82 (NGC 3034), NGC 3077 and various

dwarf galaxies, it forms a quite interesting multiple system. The central area of  $4' \times 4'$  of M 81 was searched for PNe by Jacoby et al. (1989), who discovered 185 candidate PNe. In the present paper we address the search of PNe in a much more extended region, a factor of 70 times larger than the already surveyed area, albeit with a 0.7 mag lower detection limit in the central crowded regions. Our survey covers the whole optical extent of the galaxy and its surroundings. In Sect. 2 observations and data reduction are presented. Sect. 3 contains the data analysis. In Sect. 4 we introduce the newly discovered candidate PNe, while in Sect. 5 we discuss the behaviour of their excitation in comparison with other galaxies. In Sect. 6 we build the PNe luminosity function in order to evaluate the completeness of our sample and to use it as a standard candle for extragalactic distance determination, thus deriving the corresponding distance modulus of M 81. The summary and conclusions are presented in Sect. 7.

## 2. Observations and data reduction

The M 81 galaxy was observed on December 14, 2000 and January 2, 2001 using the prime focus wide field camera (WFC) of the 2.54 m Isaac Newton Telescope (La Palma, Spain). An area of  $34' \times 34'$ , covering the whole galaxy (see Fig. 1), was surveyed with a panoramic detector consisting of four EEV CCD of  $2048 \times 4096$  pixels each. The pixel size projects to  $0''.33$  in the sky. Observations were taken through three filters with the following central wavelengths and widths (FWHM): an [O III] filter (5008/100 Å), an H $\alpha$ + [N II] filter (6568/95 Å) and a Strömgren Y filter (5550/300 Å), the latter used as an off-band filter for identifying the emission-line sources. The total exposure through the [O III] filter was of 6600 s split into two sub-exposures of 40 minutes and one of 30 minutes. The H $\alpha$ + [N II] image had a total exposure time of 1800 s (three 600 s frames) whereas the Strömgren Y image was exposed 1600 s (four 400 s exposures). The centre of the telescope pointing was: 09h 55m 33.2s, +69d 03m 55s (J2000.0). The seeing was approximately  $1''.5$  in the [O III] and *Ström. Y* frames, and  $1''$  in the H $\alpha$ + [N II] frames. The CCD frames were de-biased and flat-fielded

Send offprint requests to: M. Perinotto  
e-mail: mariop@arcetri.astro.it

\* Based on observations obtained at the 2.5m INT telescope operated on the island of La Palma by the Isaac Newton Group in the Spanish Observatorio del Roque de Los Muchachos of the Instituto de Astrofísica de Canarias.

using IRAF. All images were aligned to a reference image, correcting for geometrical distortion. Images in the same filter were then averaged out to remove cosmic rays and to improve the signal to noise ratio. Sky background was subtracted using the external regions of our frames, where the optical emission of the galaxy is negligible.

### 3. Data analysis

Emission-line objects were identified by subtracting the stellar continuum of M 81 using the off-band, *Ström*. *Y* frames from the [O III] and H $\alpha$ + [N II] frames, as described in Magrini et al. (2000). This procedure removes the stellar background allowing for identification of emission-line sources.

Following Jacoby et al. (1989), who tested the differences between crowded field photometry versus aperture photometry for the M 81 bulge PNe, we adopted the aperture photometry technique. [O III] and H $\alpha$ + [N II] line fluxes were then measured using APPHOT in the continuum-subtracted images. Errors were estimated considering both photometric errors, given by Poissonian statistics on the background and on the sources, and the detector noise. Photometric errors vary between few per cent for the brightest objects in the [O III] and H $\alpha$ + [N II] images up to about 20% for the fainter ones in the [O III] frames, whereas they can reach 50-60% for the faintest candidate PNe in the H $\alpha$ + [N II] images, where the signal to noise ratio is lower due to the shorter exposures. Instrumental fluxes were transformed into physical fluxes using the standard PN calibrator PNG 205.8-26.7, whose accurate fluxes are given in Dopita & Hua (1997).

Emission-line fluxes were then corrected for the interstellar extinction. Following Jacoby et al. (1989), we consider only the foreground Galactic extinction towards M 81, which is quoted to be  $A_V \simeq 0.3$  mag, and corresponds to  $E(B - V) \simeq 0.1$  mag (Kaufman et al. 1987). We have adopted this value to correct the [O III] and H $\alpha$ + [N II] fluxes according to Seaton (1979).

Coordinates of the emission-line sources in our images were derived with a multi-step procedure. Firstly, approximately 30 stars for each [O III] CCD field were identified on the Digitized Sky Survey<sup>1</sup>. A first astrometric solution was computed with these stars, and with this solution coordinates for about 400 stars found with DAOFIND in the field were subsequently obtained. Their coordinates were then replaced with the nearest APM-POSS1 coordinates and a new astrometric solution was computed. The procedure was iterated to reach a final accuracy of approximately 0.''5 r.m.s.

### 4. Candidate planetary nebulae

To identify PNe, we have adopted the following criteria:

- i) the object should appear both in the [O III] and H $\alpha$ + [N II] frames but not in the continuum frame. A negligible continuum is in fact expected from a PN at these wavelengths;
- ii) it should not be spatially resolved, i.e. it should have a stellar point spread function. At the distance to M 81 ( $3.50 \pm 0.40$  Mpc, Jacoby et al. 1989), 1'' corresponds to approximately 17 pc whereas the largest galactic PNe have sizes of  $\sim 4$  pc (cf. Peimbert 1990; Corradi et al. 1997). Therefore, all PNe belonging to M 81 are expected to be unresolved in our images, and any extended emission region is considered to be an H II region or a SN remnant.

One hundred and seventy-one objects fulfilling criteria i) and ii) have been found. They are listed in Table 1 together with their observed [O III] and H $\alpha$ + [N II] fluxes and coordinates; they are indicated in Fig. 1 by “+” signs. Fifty four candidates coincide with the objects discovered by Jacoby et al. (1989) in the bulge of M 81; their coordinates and fluxes agree with those in Jacoby et al. (1989) within the errors. In column 6 of Tab. 1 the identification number in Jacoby et al. (1989) is reported.

Magrini et al. (2000) have shown that the  $R = I([\text{O III}]) / I(\text{H}\alpha + [\text{N II}])$  flux ratio can be used to distinguish PNe from other emission-line objects in a statistical sense, but not for individual objects. In fact, the analysis of the catalogue of Galactic PNe by Acker et al. (1992) shows that  $R$  spans a wide range, roughly from 0 ([O III] undetected) to 10, and that  $\sim 75\%$  of PNe have  $R > 1$ . H II regions are instead generally of lower excitation ( $R < 1$ ), but this is not always true, so that misclassification between PNe and compact H II regions (which appear as point-like at the distance of M 81) can occur. Only detailed spectroscopy would allow a final distinction between the two classes of objects. Nevertheless, using the  $R$  flux ratio it is at least possible to estimate the contamination of H II regions in our sample in a statistical way, as done by Magrini et al. (2000). For the 135 objects in Table 1 in which both the [O III] and H $\alpha$ + [N II] fluxes have been measured, we find 28% with  $R < 1$ , as compared to 25% for the Galactic PNe (808 PNe whose fluxes are quoted in Acker et al. 1992). Assuming that M 81 and the Milky Way contain the same percentage of low excitation PNe, then we expect only a few H II regions (approximately 5) contaminating our sample of candidate PNe.

### 5. Radial distribution of excitation and comparison with other galaxies

The excitation class of a PN is defined in terms of flux ratios, primarily of [O III] to H $\alpha$  or H $\beta$  but also considering other nebular lines (Feast 1968). These ratios are

<sup>1</sup> Based on photographic data of the National Geographic Society Palomar Observatory Sky Survey (NGS-POSS) obtained using the Oschin Telescope on Palomar Mountain.

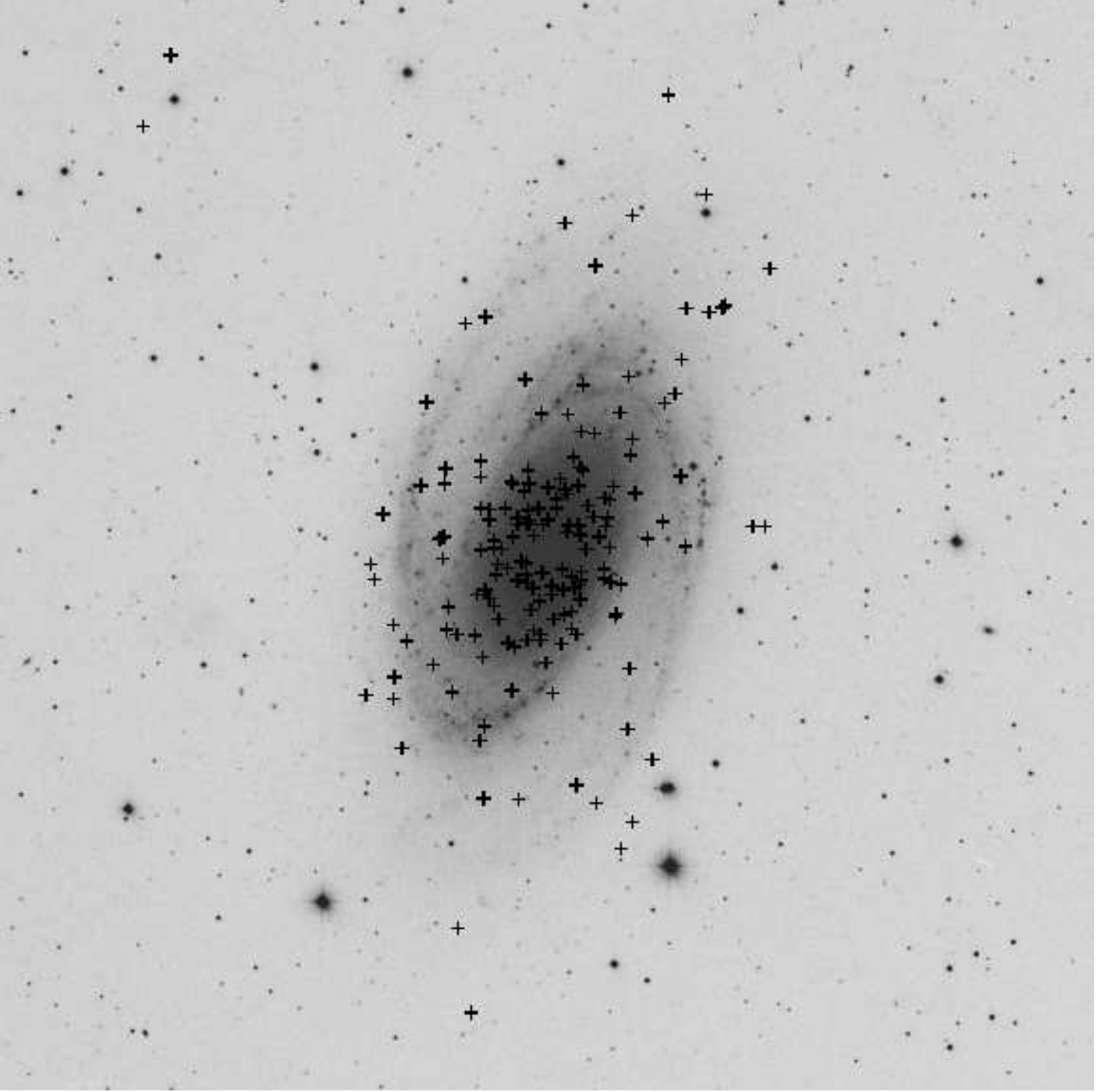


**Fig. 1.** The Palomar Atlas image of M 81. The field of this frame is approximately  $30' \times 30'$ . The field of view of the INT+WFC is slightly larger ( $34' \times 34'$ ), but we show here only the area in which we have found PNe. North is at the top, East to the left. The “+” symbols indicate the location of the candidate PNe.

good indicators of the temperature of the central star but also depend on the properties of the nebula like its geometry, electron density and temperature (and therefore the abundance of the important coolant O/H) and on the optical depth in the Lyman continuum. The flux ratio  $R = \frac{[OIII]}{H\alpha + [NII]}$  thus provides us with an indication of the excitation of the candidate PNe in M 81, as already anticipated in the previous section.

In the Galaxy, Vorontsov-Vel'yaminov et al. (1975) presented an absolute spectrophotometry of 47 PNe in the direction of the Galactic centre. They found that their  $R$  ratios differ significantly from those of disk PNe, concluding that there are physical differences between Galactic bulge and disk PNe. Webster (1975, 1976) compared the distribution of excitation of the Galactic bulge PNe with those in the Magellanic Clouds and proposed the presence

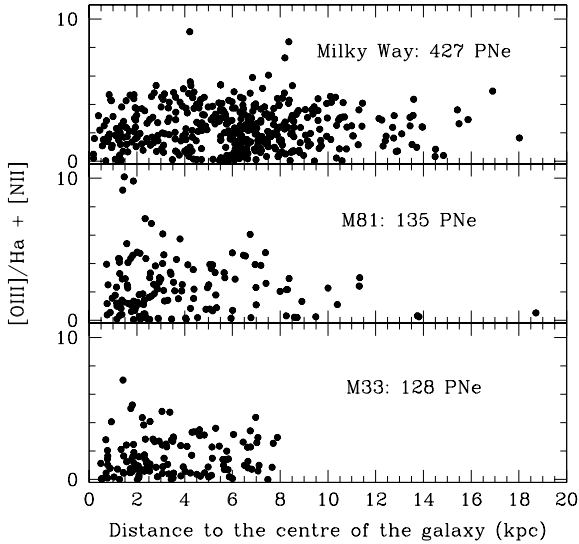


**Fig. 2.** The flux ratio  $R = \frac{[\text{O III}]}{H\alpha + [\text{N II}]}$  as a function of the galactocentric distance for the Milky Way (data from Acker et al. 1992, upper box), M 81 (this work, middle box), and M 33 (Magrini et al. 2000, Magrini et al. 2001, lower box).

of more massive progenitors in the case of LMC, where there are more high excitation PNe than low excitation ones, compared to our Galaxy and the SMC. In spiral galaxies, information on the excitation of PNe thorough the bulge and the disk is available only for M 81 (this paper), M 33 (Magrini et al. 2000) and the Galaxy (Acker et al. 1992). Using the information contained in the Strasbourg ESO Catalogues, the galactocentric distances of 427 Galactic PNe with quoted  $H\alpha$ ,  $[\text{N II}]$  and  $[\text{O III}]$  fluxes were computed; the distances from the Sun of the PNe come from Cahn et al. (1992), and the adopted galactocentric distance of the Sun is  $8.5 \pm 1.1$  kpc (Allen, 2000).

Fig. 2 shows  $R$  as a function of the distance from the centre of the galaxy in the three cases. PNe in M 33 and the Milky Way are approximately homogeneously distributed in terms of excitation. The apparent progressive reduction of high excitation PNe with galactocentric distance in M 81 (Fig. 2) is removed if the mean  $R$ , computed in bins of 2 kpc, is plotted (Fig. 3).

Therefore, and contrary to Vorontsov-Vel’yaminov et al. (1975), no significant difference between the excitation of bulge and disk PNe is found in the Galaxy nor in M 81 (Fig. 4).

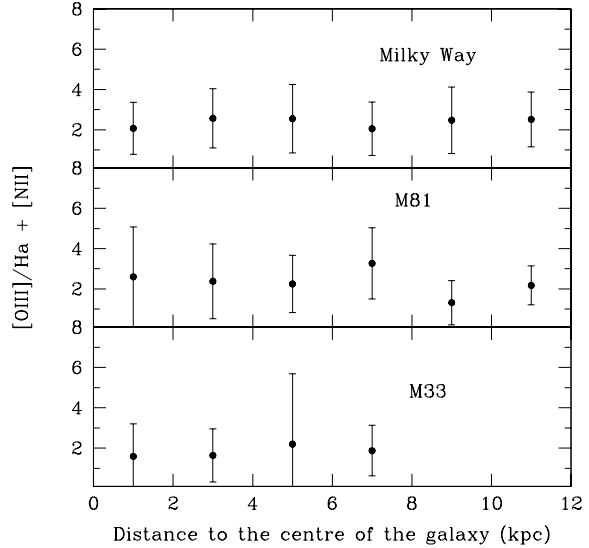


**Fig. 3.** As in Fig.2, but plotting the mean value of  $R$ , averaged on bins of 2 kpc and up to the distance of 12 kpc. The error bars indicate the standard deviation from the mean.

## 6. Planetary Nebulae Luminosity Function

$[\text{O III}]$  fluxes for the candidate PNe in M 81 were converted into equivalent V-band magnitudes following Jacoby (1989):

$$m_{[\text{O III}]} = -2.5 \log F_{[\text{O III}]} - 13.74. \quad (1)$$

The Planetary Nebulae luminosity function (PNLF) was then built for three different samples: all 171 PNe of M 81, those in the disk (86 objects) and those in the bulge (85). They are presented in Fig. 5. The Eddington formula (Eddington 1913) was applied to correct for the effects of observational errors. The resulting luminosity function within the completeness limit was then fit to the “universal” PNLF

$$N(m) \propto e^{0.307(m)}(1 - e^{3(m_* - m)}). \quad (2)$$

In Eq. (2)  $m$  is the observed  $[\text{O III}]$  magnitude from Eq. (1), and  $m_*$  is the apparent magnitude of the PNLF cutoff of M31 (Jacoby 1989). As we have discussed in Magrini et al. (2000), it is possible to estimate the limit of completeness of a sample of PNe by computing the S/N ratio for each PNe (putting the limit of completeness at  $S/N \sim 10$ , Ciardullo et al. (1987)) or equivalently by evaluating the point at which observational PNLFs inflect downwards indicating incompleteness. Fig. 5 shows that the completeness limit changes for the different samples, indicating the strong dependence on the galaxian background emission, which increases towards the centre of the galaxy. Comparing our data with the sample of Jacoby et al. (1989), we note in fact that we are losing approximately 70% of

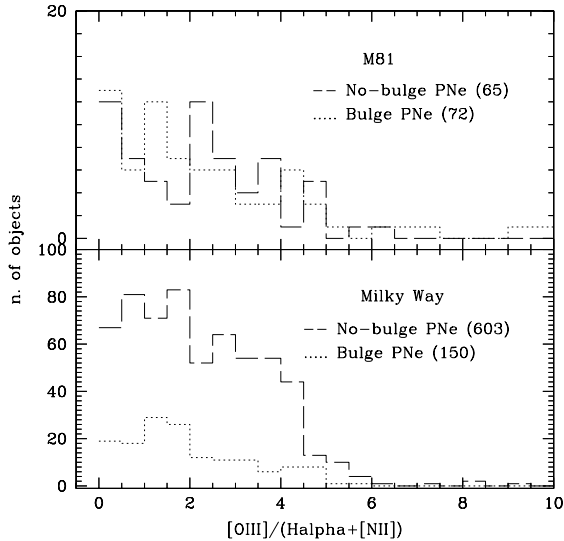


**Fig. 4.** Histograms of R for M 81 (this work, upper box) and the Milky Way (lower box), for disk and bulge PNe separately.

the PNe found by Jacoby and collaborators in the bulge of M 81. This is due to two effects: the use of a filter that is three times broader than the one used by Jacoby et al. (1989), and a smaller primary mirror (2.5 m vs. 4 m) not compensated by longer exposure times (1.8 hr vs. 1.5 hr). These effects are particularly important in the central regions because of the high surface brightness of the parent galaxy. In these regions our completeness limit of 24.0 mag differs from that of the sample of Jacoby et al. (24.7 mag) and from the one we have for our data in the disk (24.7 mag). For this reason the distance modulus of M 81 is computed using only disk PNe, where we consider to have a complete sample. The error on the distance modulus is obtained by combining the error associated with our best least mean square fits ( $\pm 0.04$  mag) in quadrature with those associated with the photometric zero point (0.03 mag) and with the adopted extinction (0.2 mag from Kaufman et al. 1987). We have also to consider two systematic errors which come from the uncertain definition of the empirical PNLF (0.05 mag) and the distance of the calibration galaxy M31 (0.10 mag). These errors lead to a total error of  $\pm 0.23$  mag. The resulting distance modulus to M 81 is  $27.92 \pm 0.23$  mag, corresponding to  $3.84 \pm 0.41$  Mpc. This distance is in excellent agreement with the value derived from the Cepheids method of  $27.97 \pm 0.14$  mag (Huterer et al. 1995) and also in fair agreement with the value derived by Jacoby et al. (1989) using the luminosity function for their bulge PNe candidates ( $27.72 \pm 0.25$  mag).

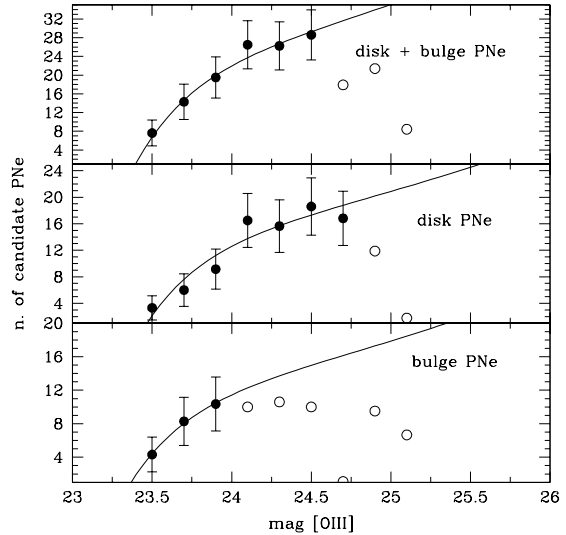


**Fig. 5.** Mean square fits for the luminosity functions of PNe in M 81: i) Complete sample (171 candidate PNe); ii) Disk (86 candidate PNe); iii) Bulge and central regions (85 candidate PNe). Black points indicate candidate PNe within the completeness limits.

## 7. Summary and conclusions

We imaged a  $34' \times 34'$  area around the spiral galaxy M 81 through [O III] and  $H\alpha + [N II]$  narrowband filters. In total, 171 candidate PNe are found, 117 of which are new while 54 coincide with those discovered by Jacoby et al. (1989) in the central  $4' \times 4'$  bulge.

The behaviour of PNe excitation across the galaxy was examined, finding no evidence for substantial differences in excitation between bulge and disk PNe, nor for variations along the galaxian disk. The same result applies to the Milky Way and M 33, and is contrary to previous suggestions from Vorontsov-Vel'yaminov et al. (1975).

The PNLF of the candidate PNe in the disk of M 81 provides a distance determination of  $3.84 \pm 0.41$  Mpc.

*Acknowledgements.* We are grateful to Peter Sorensen for taking the observations of M 81 in service mode.

## References

- Acker A., Ochsenbein F., Stenholm B., Tyllenda R., Marcout J., Schon C., *Strasbourg-ESO Catalogue Of Galactic Planetary Nebulae*, 1992.
- Allen C. W. 2000, *Allen's Astrophysical quantities*, London.
- Aller L.H., Liller W. 1968 in *Nebulae and Interstellar matter* Page. 483-569, University of Chicago Press.
- Cahn J. H., Kaler J. B., Stanghellini, L. 1992, *A&AS*, 94, 399.
- Ciardullo, R., Ford, H. C., Neill, J. D., Jacoby, G. H., Shafter, A. W. 1987, *Apj*, 318, 520.

- Corradi, R.L.M., Villaver, E., Mampaso, A., Perinotto, M. 1997, *A&A* 324, 276
- Dopita, M.A. & Hua, C.T. 1997, *ApJS*, 108, 105.
- Eddington, A. S. 1913, *M.N.R.A.S.*, 73, 359.
- Feast, M.W. 1968, *MNRAS*, 140, 345.
- Feldmeier J. J., Ciardullo R., Jacoby G. H. 1997, *ApJ*, 479, 231.
- Huterer D., Sasselov D. D., Schechter P. L. 1995 *AJ*, 110, 2705.
- Jacoby G. H. 1989 *ApJ* 1989*ApJ*, 339, 39.
- Jacoby G. H., Ciardullo R., Holland C. F., Booth F. 1989 *ApJ*, 344, 704.
- Jacoby, G. H. 1997, in *Planetary nebulae*, IAU Symp. N. 180, H. J. Habing and H. J. G. L. M. Lamers eds, Dordrecht, Kluwer, p. 448.
- Kaufman M., Bash F. N., Kennicutt R. C., Hodge P. W. 1987,*ApJ*, 319, 61.
- Magrini L., Corradi R. L. M., Mampaso A., Perinotto M. 2000, *A&A*, 355, 713.
- Magrini L., Cardwell A., Corradi R. L. M., Mampaso A., Perinotto M. 2001, *A&A*, 367, 498.
- Peimbert, M. 1990, *Rep. Prog. Phys.*, 53, 1559
- Seaton M. J. 1979, *MNRAS*, 187, 73.
- Vorontsov-Vely'aminov B. A., Kostyakova E. B., Dokuchaeva O. D., Arkhipova V. P. 1975 *Astronomicheskii Zhurnal*, 52, 264.
- Webster B. L. 1975 *MNRAS*, 173, 437.
- Webster B. L. 1976 *MNRAS*, 174, 513.

**Table 1.** PN candidates found in M81. Fluxes in  $H\alpha + [N\ II]$  and in  $[O\ III]$  are in units of  $10^{-16}$  erg  $cm^{-2}$   $s^{-1}$  and are corrected for reddening (see text).

id	R.A. (2000.0)	Dec.	$F_{[OIII]}$	$F_{H\alpha}$	Jacoby id	id	R.A. (2000.0)	Dec.	$F_{[OIII]}$	$F_{H\alpha}$	Jacoby id
1	9 54 20.35	69 03 53.7	2.9	0.64		86	9 55 37.78	69 00 31.7	7.8	2.4	
2	9 54 24.35	69 03 56.0	3.0	–		87	9 55 37.98	69 02 21.4	5.5	4.6	
3	9 54 26.54	69 10 30.5	5.5	25.		88	9 55 38.12	69 04 47.3	3.9	2.5	121
4	9 54 27.66	69 13 55.0	5.3	2.2		89	9 55 38.62	69 04 42.1	7.1	–	126
5	9 54 31.12	69 10 25.8	4.1	1.9		90	9 55 38.63	69 05 06.8	7.9	2.4	124
6	9 54 36.70	69 17 00.5	5.6	22.		91	9 55 38.65	69 01 23.3	4.5	–	
7	9 54 38.52	69 10 36.8	4.9	2.4		92	9 55 39.04	69 01 12.3	6.9	1.8	
8	9 54 45.50	69 08 06.6	7.6	1.6		93	9 55 39.07	69 05 42.1	13.	250.	
9	9 54 46.52	69 05 39.0	11.	56.		94	9 55 39.51	69 02 46.7	12.	35.	
10	9 54 49.97	69 04 10.5	6.3	2.5		95	9 55 39.77	69 04 43.1	7.2	–	131
11	9 54 53.15	69 13 32.2	5.0	2.2		96	9 55 40.31	69 04 53.7	3.4	2.8	133
12	9 54 54.24	69 04 21.0	6.7	2.5		97	9 55 40.70	69 01 30.1	3.4	2.1	
13	9 54 59.90	69 03 53.6	3.5	1.2		98	9 55 41.00	69 03 32.1	10.	4.0	136
14	9 54 09.28	69 11 31.0	4.0	3.6		99	9 55 41.11	69 02 08.9	4.2	6.0	137
15	9 55 01.01	69 12 04.3	5.3	1.8		100	9 55 41.20	69 02 56.3	9.2	7.9	
16	9 55 01.47	69 06 54.1	4.3	1.1		101	9 55 41.69	69 03 11.0	4.6	–	139
17	9 55 10.09	69 02 37.1	6.4	70.		102	9 55 42.23	69 04 54.3	8.2	1.9	143
18	9 55 10.25	69 00 05.3	3.7	2.4		103	9 55 42.50	69 04 42.6	6.0	–	144
19	9 55 11.18	69 05 09.9	5.3	0.7	4	104	9 55 42.58	69 03 36.9	10.	18.	
20	9 55 12.24	69 04 37.8	5.0	3.9	5	105	9 55 42.74	69 05 56.8	5.5	–	145
21	9 55 12.47	69 05 13.6	4.9	4.4	11	106	9 55 43.21	69 06 01.5	3.8	8.5	
22	9 55 12.65	69 01 46.2	7.5	3.4		107	9 55 43.39	69 01 16.1	6.3	–	
23	9 55 12.73	69 03 46.0	3.9	2.9	12	108	9 55 44.36	69 03 03.4	5.5	–	152
24	9 55 13.12	69 04 22.7	5.2	–	14	109	9 55 44.50	69 04 21.4	5.3	3.0	153
25	9 55 13.35	68 58 16.8	7.1	48.		110	9 55 45.97	69 05 13.6	5.7	5.1	158
26	9 55 13.39	69 01 40.8	5.0	–		111	9 55 46.25	69 06 21.5	7.3	–	
27	9 55 13.58	69 02 43.0	7.2	84.		112	9 55 47.62	69 01 05.4	2.0	0.95	
28	9 55 13.62	69 07 10.3	8.7	–		113	9 55 47.72	69 03 27.7	7.0	17.	164
29	9 55 14.78	68 55 30.0	12.	38.		114	9 55 48.42	69 02 19.8	5.6	3.1	169
30	9 55 15.65	69 02 48.9	3.9	–	19	115	9 55 48.61	69 04 02.6	4.0	2.8	
31	9 55 15.65	69 04 06.3	6.7	2.7		116	9 55 49.70	69 01 13.5	9.2	2.3	
32	9 55 15.70	69 08 39.8	6.5	2.6		117	9 55 50.11	68 59 48.4	7.7	3.5	
33	9 55 15.96	69 13 31.7	6.1	24.		118	9 55 50.50	69 03 34.2	5.4	1.0	177
34	9 55 16.93	69 04 42.9	5.7	–	23	119	9 55 50.96	69 04 18.8	6.1	1.5	180
35	9 55 18.39	69 05 04.2	5.6	9.0	27	120	9 55 51.34	69 04 04.9	6.6	2.9	181
36	9 55 18.97	69 06 08.0	6.0	1.8		121	9 55 51.46	69 05 14.9	12.	44.	
37	9 55 19.41	69 06 12.2	4.5	–		122	9 55 51.56	68 56 33.0	5.8	1.5	
38	9 55 19.47	68 54 45.7	5.6	4.2		123	9 55 51.61	69 03 18.4	7.0	1.6	183
39	9 55 19.55	69 03 54.6	5.2	–		124	9 55 51.73	69 04 56.3	2.9	3.4	182
40	9 55 02.48	69 05 17.0	7.3	1.2		125	9 55 52.14	69 01 57.0	6.1	3.6	
41	9 55 02.58	69 06 26.3	9.9	6.5		126	9 55 52.49	69 06 43.3	4.1	2.9	
42	9 55 20.53	69 03 45.9	9.7	99.		127	9 55 52.93	69 10 52.1	4.6	4.2	
43	9 55 20.80	69 05 41.7	6.6	–	30	128	9 55 53.02	69 06 15.2	6.7	2.5	
44	9 55 21.53	69 06 33.0	8.5	3.7		129	9 55 53.30	69 02 21.6	10.	2.3	
45	9 55 21.81	69 07 50.6	9.1	120.		130	9 55 54.29	69 05 18.6	11.	24.	
46	9 55 22.14	69 04 13.0	9.3	–	35	131	9 55 54.66	69 02 37.5	5.3	3.7	
47	9 55 22.40	69 04 30.5	4.9	2.1		132	9 55 55.62	69 02 53.2	5.4	2.9	
48	9 55 22.81	69 03 05.8	9.4	2.3	37	133	9 55 55.69	69 04 03.6	4.3	–	
49	9 55 23.38	69 02 50.9	11.	1.2	39	134	9 55 58.53	69 02 45.8	8.4	2.8	
50	9 55 24.04	69 02 43.4	10.	0.99	42	135	9 55 58.78	69 00 53.1	6.3	1.1	
51	9 55 24.40	69 02 17.9	4.6	–	46	136	9 55 06.11	68 57 18.5	4.6	0.76	
52	9 55 24.48	69 03 37.9	6.3	–	45	137	9 55 07.29	69 12 10.4	5.2	2.4	
53	9 55 24.99	69 05 01.2	8.3	9.8	48	138	9 55 09.25	69 05 32.1	7.1	2.8	
54	9 55 25.01	69 05 28.4	9.4	–	49	139	9 56 00.46	68 58 50.0	5.7	1.7	
55	9 55 25.43	69 05 37.8	9.8	1.0	50	140	9 56 00.56	69 01 33.9	6.1	1.8	
56	9 55 25.52	69 04 31.6	7.4	–	52	141	9 56 01.77	69 01 24.6	2.7	1.3	
57	9 55 25.65	69 02 39.6	4.4	3.4	54	142	9 56 13.41	69 06 10.6	5.3	6.3	
58	9 55 26.30	69 04 20.3	9.7	25.	56	143	9 56 14.30	68 50 20.5	6.1	19.	
59	9 55 26.38	69 02 59.8	4.2	–		144	9 56 15.41	69 00 48.8	3.2	4.1	
60	9 55 26.66	69 05 56.1	8.6	–	57	145	9 56 15.92	68 52 54.1	3.3	1.1	
61	9 55 26.84	69 01 16.6	11.	5.9		146	9 56 02.41	68 58 24.8	5.8	2.0	
62	9 55 27.64	69 01 57.7	5.1	–		147	9 56 20.74	68 58 26.8	5.5	1.4	
63	9 55 28.25	69 01 26.5	6.3	93.		148	9 56 23.37	69 01 35.2	5.8	7.3	
64	9 55 28.56	69 05 22.0	4.1	1.4	67	149	9 56 27.09	69 05 26.4	11.	2.8	
65	9 55 29.13	69 05 04.0	7.9	–	71	150	9 56 27.29	69 02 51.4	4.6	2.0	
66	9 55 29.20	69 03 15.2	8.1	–	76	151	9 56 27.30	69 02 07.0	4.3	1.1	
67	9 55 29.60	69 02 38.6	6.6	–	79	152	9 56 28.38	68 58 25.6	9.9	3.8	
68	9 55 30.24	69 01 53.7	6.7	5.9		153	9 56 28.70	69 00 32.8	12.	17.	
69	9 55 30.45	69 03 34.1	10.	–		154	9 56 29.82	68 59 55.3	5.5	1.2	
70	9 55 30.62	69 07 56.3	11.	67.		155	9 56 03.09	68 56 39.7	4.0	0.84	
71	9 55 31.36	69 05 44.4	5.5	1.2	82	156	9 56 03.73	69 08 27.0	3.4	1.9	
72	9 55 31.95	68 56 47.5	6.2	33.		157	9 56 31.99	69 03 31.3	7.4	2.2	
73	9 55 32.14	69 01 02.7	9.5	67.		158	9 56 32.84	69 03 58.8	6.5	7.3	
74	9 55 32.27	69 04 46.6	6.3	–	86	159	9 56 38.50	69 00 07.0	3.7	1.6	
75	9 55 33.34	69 02 46.0	4.3	4.3	94	160	9 56 04.48	69 06 36.0	6.0	2.9	
76	9 55 33.61	69 02 32.7	9.9	3.4		161	9 56 05.45	69 06 10.3	6.0	1.4	
77	9 55 33.68	69 01 48.1	5.2	1.1		162	9 56 06.20	69 03 54.3	4.8	1.6	
78	9 55 34.02	69 04 39.2	7.5	1.9	97	163	9 56 06.53	69 01 36.9	5.7	–	
79	9 55 34.58	69 09 00.9	5.1	1.4		164	9 56 07.50	69 04 33.6	6.0	1.3	
80	9 55 34.97	69 05 08.6	6.1	1.4	100	165	9 56 08.31	69 02 29.0	3.4	37.	
81	9 55 36.02	69 03 13.0	7.3	6.2	107	166	9 56 08.41	69 08 37.8	5.1	1.7	
82	9 55 36.26	69 02 45.1	13.	–		167	9 56 08.54	69 03 56.0	4.9	3.6	
83	9 55 36.81	68 59 35.3	10.	2.8		168	9 56 09.03	69 04 32.2	4.9	–	
84	9 55 37.13	69 05 53.8	4.8	1.0	111	169	9 56 09.87	68 59 56.0	5.6	8.3	
85	9 55 37.17	69 06 18.1	12.	82.		170	9 56 09.89	69 01 47.9	8.1	–	
						171	9 57 23.75	69 19 41.6	9.5	18.	